JOURNAL OF SYNCHROTRON RADIATION
ISSN 1600-5775

Received 29 November 2014
Accepted 15 March 2015

Edited by I. Schlichting, Max Planck Institute for Medical Research, Germany

Keywords: lasers; free-electron lasers; coherence.

The FERMI free-electron lasers

E. Allaria,[a] L. Badano,[a] S. Bassanese,[a] F. Capotondi,[a] D. Castronovo,[a] P. Cinquegrana,[a] M. B. Danailov,[a] G. D'Auria,[a] A. Demidovich,[a] R. De Monte,[a] G. De Ninno,[a,c] S. Di Mitri,[a] B. Diviacco,[a] W. M. Fawley,[a] M. Ferianis,[a] E. Ferrari,[a,b] G. Gaio,[a] D. Gauthier,[a] L. Giannessi,[a,d]* F. Iazzourene,[a] G. Kurdi,[a] N. Mahne,[a] I. Nikolov,[a] F. Parmigiani,[a,b] G. Penco,[a] L. Raimondi,[a] P. Rebernik,[a] F. Rossi,[a] E. Roussel,[a] C. Scafuri,[a] C. Serpico,[a] P. Sigalotti,[a] C. Spezzani,[a] M. Svandrlik,[a] C. Svetina,[a,b] M. Trovó,[a] M. Veronese,[a] D. Zangrando[a] and M. Zangrando[a,e]

[a]Elettra-Sincrotrone Trieste, Trieste, Italy, [b]University of Trieste, Trieste, Italy, [c]Nova Gorica University, Nova Gorica, Slovenia, [d]ENEA CR Frascati, Frascati, Italy, and [e]IOM-CNR, Laboratorio TASC, Trieste, Italy.
*Correspondence e-mail: luca.giannessi@elettra.eu

FERMI is a seeded free-electron laser (FEL) facility located at the Elettra laboratory in Trieste, Italy, and is now in user operation with its first FEL line, FEL-1, covering the wavelength range between 100 and 20 nm. The second FEL line, FEL-2, a high-gain harmonic generation double-stage cascade covering the wavelength range 20–4 nm, has also completed commissioning and the first user call has been recently opened. An overview of the typical operating modes of the facility is presented.

1. Introduction

FERMI is a fourth-generation light source at the Elettra laboratory in Trieste, Italy (Bocchetta *et al.*, 2007). It is a 350 m-long straight machine hosted in three main buildings, close to the Elettra storage ring. Fig. 1 shows the site with Elettra (E) and other supporting buildings, where in the bottom part, from right to left, one can see the 200 m Linac building (1), the 100 m Undulator Hall (2) and the 60 m Experimental Hall (3). Building (4) contains plants for conventional utilities.

The facility hosts two single-pass separate free-electron lasers (FELs) using the same accelerator complex. The scientific case driving the design of the FELs is based on multiple experimental programs, with three beamlines already in operation and an additional three whose construction is foreseen in the near future. The experiments require high peak brightness, fully coherent, narrow and stable bandwidth photon pulses, wavelength tunability and variable polarization: circular and linear. Both FERMI FELs are externally seeded to produce photons with high temporal coherence and wavelength stability in the ultraviolet and soft X-ray range, between 12 eV and 310 eV (Allaria *et al.*, 2012*a*, 2013*a*). The low-energy FEL, FEL-1, reaches up to 62 eV and is based on a single-stage high-gain harmonic generation (HGHG) scheme (Yu *et al.*, 2000), with a modulator undulator and a radiator with six undulator elements. The high-energy FEL line, FEL-2, generates photons down to 4 nm wavelength in the fundamental and 1.3 nm in the third harmonic and is based on a double-stage HGHG cascade, where the first stage is made by a modulator undulator and two radiator modules, and the second stage by a modulator undulator and six radiator modules. FEL-2 utilizes the fresh bunch injection technique

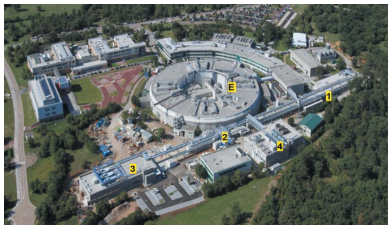

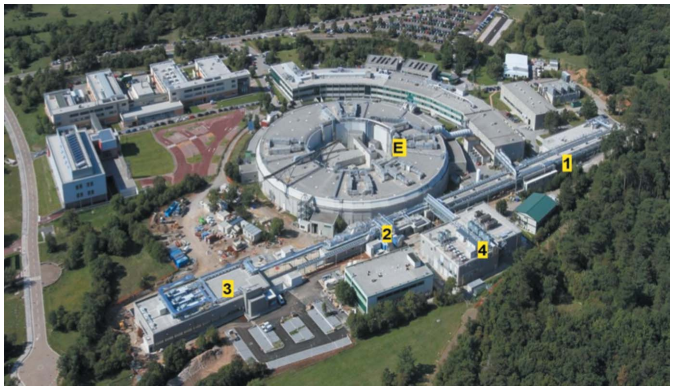

Figure 1
Aerial view of the Elettra-Sincrotrone Trieste facilities: FERMI and Elettra.

configuration (Ben-Zvi *et al.*, 1992). In this set-up the free-electron laser is configured as a two-stage cascade, where the second stage is seeded by the light produced by the first stage. The photons in the second stage are generated from a fresh portion of the electron bunch, which has not been heated by the seed of the first stage, overcoming the problem of the induced energy spread which limits the order of the harmonic conversion in a high-gain harmonic generation seeded FEL.

FEL-1 started operation for users in December 2012 and since then has welcomed scientists from Italy and from all over the world to perform experiments on the three experimental stations so far available, namely the Diffraction Projection Imaging (DiProI) station (Capotondi *et al.*, 2013, 2015), the Elastic Inelastic Scattering TIMEX (EIS-TIMEX) station (Masciovecchio *et al.*, 2015) and the Low Density Matter (LDM) station (Svetina *et al.*, 2015). FEL-2 produced the first coherent photons at 14.4 nm in October 2012; that was the first experimental demonstration of a seeded free-electron laser configured as a two-stage cascade operating in the 'fresh bunch injection' mode. Since then, FEL-2 commissioning runs were performed in between user operation runs on FEL-1. This allowed steady extension of the operating range of FEL-2, until the nominal performance at 4 nm was attained in June 2014. The first call for external user proposals for FEL-2 was recently issued in fall 2014.

2. FERMI FEL-1

A schematic layout of FERMI FEL-1 is shown in Fig. 2. In the first undulator (the Modulator in the figure) the interaction of the beam with an external laser induces an energy modulation with the periodicity of the laser wavelength. The energy

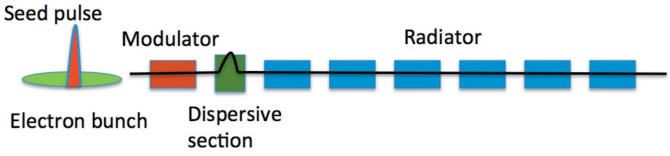

Figure 2
Layout of FERMI FEL-1.

modulation is then converted into a density modulation by a dispersive magnet, a small chicane where the electron path length depends on the particle energy. The density modulation is not purely sinusoidal and contains higher-order harmonic components. For this reason, when the beam is injected into the final radiator, composed of six undulator modules, with the resonance tuned at one of the higher harmonics of the modulator, the FEL amplification process is not initiated by the e-beam shot noise as in a self-amplified spontaneous emission (SASE) FEL (Kondratenko & Saldin, 1980; Sprangle *et al.*, 1980; Haus, 1981; Dattoli *et al.*, 1981; Bonifacio *et al.*, 1984) but from the induced density modulation, which retains the phase and amplitude information of the seed laser.

There are several advantages correlated to this configuration, such as coherence length, stable central frequency and very good synchronization with an external laser. The FEL pulse has indeed a coherence length comparable with the pulse length and the output radiation spectrum is not composed of the random superposition of spikes centered at the resonant frequency as in a SASE FEL, but is a single-mode structure close to the Fourier limit, whose width is related to the overall pulse length. The central frequency of the emitted light at the lowest order is determined by the seed laser frequency scaled by the harmonic order and is not affected by fluctuations of the electron beam energy (Allaria *et al.*, 2012*b*). Since the electron beam is longer than the seed pulse, the synchronization with an external optical laser is not affected by the electron beam jitter and the FEL pulse arrival time is determined by the arrival time of the seed laser pulse. Due to the intrinsic synchronization of the FEL with the seed laser, pump and probe experiments with a jitter as low as 6 fs (r.m.s.) were accomplished by transporting the seed laser to the experimental stations (Danailov *et al.*, 2014). Here the main source of timing jitter is the optical beam transport over a distance of 150 m, whose contribution is estimated to be less than 5 fs (r.m.s.).

The wavelength of the FEL radiation can be varied by tuning the seed wavelength together with the undulator resonance. The latter is controlled through the variable undulator gap, which can be closed down to 10 mm. FEL-1's nominal output wavelength range extends from 100 nm down to 20 nm. Another unique feature of FERMI is that the radiators of both the FEL amplifiers, FEL-1 and FEL-2, are APPLE-II undulators (Sasaki, 1994). This choice allows us to change the polarization of the emitted light from purely linear to purely circular (Allaria *et al.*, 2014). This capability of variable polarization is an important and attractive feature, as it gives access to new areas of science that cannot be explored with linearly polarized light (Eisebitt *et al.*, 2004; Bigot *et al.*, 2009; Janssen & Powis, 2014; Garcia *et al.*, 2013; Tia *et al.*, 2013; Spezzani *et al.*, 2011). The operating conditions of the FEL, as pulse energy, wavelength, spectral width and polarization, and in some cases the generation of multiple pulses for pump and probe experiments, can be adapted to a specific experimental setup. The time for optimization and fine tuning of the FEL strongly depends on the setup requested by the users, but for the standard operating conditions of FEL-1 the operability

and reliability of the machine results in an uptime close to 90%.

2.1. The seed laser system

A broadly tunable deep-UV laser system (230–300 nm wavelength range) with a peak power in excess of 100 MW is needed in order to induce sufficient bunching in the spectral range of operation of the FERMI FELs. The seed pulse duration depends on the specific setup used and typically varies in the 100–200 fs range. An energy per pulse of 10–20 μJ of UV reaching the modulator is required, with larger values needed specifically for FEL-2 in the wavelength interval between 4 and 5 nm. These requirements are successfully met by a commercial parametric amplifier (Light Conversion/Coherent Opera Solo) pumped by a 6.5 mJ femtosecond regenerative amplifier (Coherent Elite) followed by a single-pass amplifier stage. The signal- and idler-wavelengths of the OPA span from 1.08 μm to about 2.6 μm and the final frequency conversion to the UV is achieved through nonlinear harmonic generation and mixing.

The FEL can also be seeded at fixed wavelength with the third harmonic of the Ti:Sa laser system. In this case a larger seed energy per pulse is available with higher phase uniformity. This results in the possibility of reaching higher harmonic conversion factors in the FEL, with a typically narrower spectral line-width.

2.2. Spectral properties and performances

FEL-1 is characterized by a high stability of the output central wavelength, typically better than 10^{-4} r.m.s. The output spectral stability and pulse energy from FEL-1 were extensively discussed by Allaria *et al.* (2012*a*,*b*). We report here on the most recent improvements related to this source, including the extension of the operation range at wavelengths shorter than 20 nm. These improvements were possible because of the careful tuning of the linac system including the X-band linearizer and the laser heater, to produce a moderate peak current (*e.g.* 700 A) beam with a good longitudinal phase space (Penco *et al.*, 2014). When the seed is generated by the Optical Parametric Amplifier laser system (OPA mode), the FEL is continuously tunable. However, the FEL tuning range of 100–20 nm is covered with different machine setups including the optimization of the specific OPA non-linear process and electron beam energy. Typical tuning ranges available during a single user beam-time are 65–20 nm or 100–30 nm with some restrictions depending on the combination of the OPA tuning range and FEL harmonic order. A summary of the FEL-1 source parameters is listed in Table 1.

The best output pulse energy performance and spectral quality ($\Delta\lambda/\lambda < 5 \times 10^{-4}$ r.m.s.) are available when the FEL is seeded at fixed wavelength, at the third harmonic of the Ti:sapphire amplifier (261.6 nm, THG mode). In this case only integer harmonics of the constant seed wavelength are available. In Fig. 3 we show the typical FEL spectra at the 6th and 11th harmonics of the seed (right panel) as measured by the spectrometer PRESTO (Zangrando *et al.*, 2009). PRESTO is a non-destructive diagnostic based upon a grating that deflects the higher orders of diffraction, while simultaneously delivering the zero-order of reflection, with more than 97% of the FEL pulse energy, to the experimental stations. A CCD monitors the spectrum from the dispersed higher orders with the control system tagging the data with a unique bunch number identifier, thus allowing the users to correlate on a pulse-by-pulse basis their own data results with the FEL spectral properties.

Table 1
List of the main parameters of FEL-1.

Beam energy (GeV)	1.0–1.5
Peak current (A)	500–700
Wavelength range (nm)	100–20
Polarization	Variable
Expected pulse length (fs)	<100
Energy per pulse (μJ)	∼100 (in circular polarization)
Repetition rate (Hz)	10–50
Typical relative bandwidth (%, r.m.s.)	$\lesssim 0.05$
Typical shot-to-shot stability (%, r.m.s.)	∼10%

The spectral images were extracted from a set of 420 consecutive shots, and the histogram in the left frame in Fig. 3 shows the distribution of the relative spectral width of the entire set of data at 43.6 nm. The average relative spectral bandwidth is 0.035% (r.m.s.). A similar value is obtained at 23.8 nm.

For comparison, in Fig. 4 the FEL spectrum with the seed generated by the OPA laser is shown (left frame). In this case the FEL is in linear-vertical polarization mode, the seed wavelength is about $\lambda_{seed} = 246$ nm and the radiator is tuned at 24.6 nm, corresponding to the 10th harmonic of the seed. The right-hand frame shows a sequence of 330 stacked spectra. Each horizontal line represents the spectral profile of a single

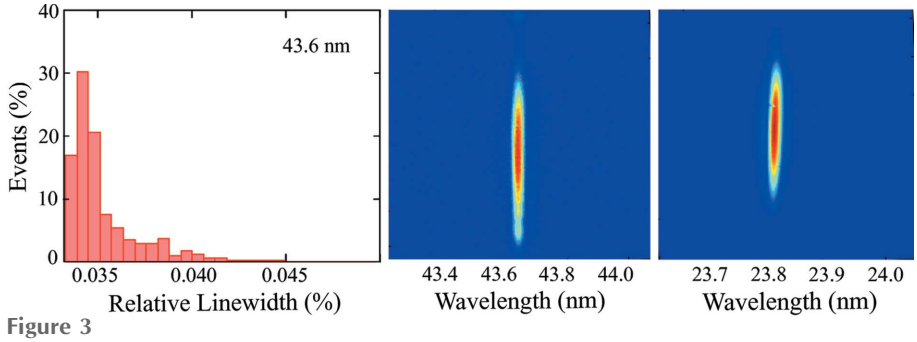

Figure 3
(Left) Histogram of the FEL relative line-width at 43.6 nm (statistics over a sequence of 420 spectra). (Center and right) Single-shot spectral images from the spectrometer CCD at 43.6 nm and 23.8 nm, respectively, of the 6th and 11th harmonics of the seed (THG mode). The images show the intensity as a function of wavelength on the horizontal axis. The vertical axis maps the vertical shape of the FEL intensity distribution at the spectrometer. The average relative bandwidth (r.m.s.) is about 0.035% at 43.6 nm and 0.037% for a similar sequence at 23.8 nm. The average energy per pulse in these two sets of data was 80 μJ (43.6 nm) and 60 μJ (23.8 nm) with an r.m.s. standard deviation of about 10 μJ in both cases.

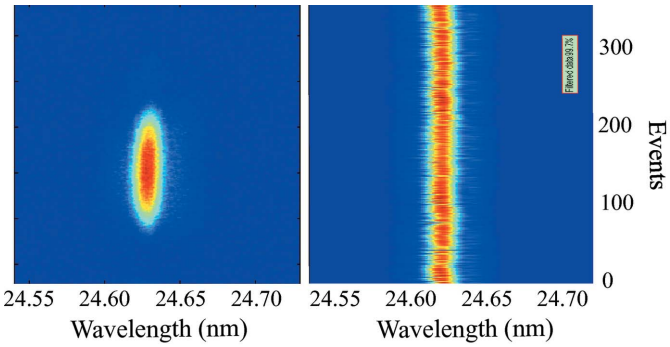

Figure 4
(Left) As in Fig. 3, spectral image of FEL-1 at 24.6 nm, corresponding to the 10th harmonic of the seed at 246 nm. (Right) Sequence of 330 stacked spectra (OPA mode). Each horizontal line represents the spectral profile of a single shot projected onto the horizontal (frequency) axis.

shot projected on the horizontal (frequency) axis. The sequence was acquired in optimized conditions and the figure shows the remarkable central wavelength and spectral shape stability. The average line-width of the sequence is 0.032%. In this example the OPA-generated seed provided a spectral quality comparable with the one typically available with the THG seed.

The average energy per pulse in the sequence displayed in Fig. 4 was about 90 μJ with a standard deviation of about 7%. Typical energy per pulse in the range 20–100 μJ is available. The upper limit depends on the operation wavelength and polarization state. A factor of two or more energy may be available by partially relaxing the condition on spectral purity.

Despite the lower limit of the nominal wavelength range of operation of FEL-1 being 20 nm, the 13th harmonic of the THG seed, the FEL has demonstrated adequate properties for exploiting experiments even at higher harmonic orders. As an example, Fig. 5 shows a sample spectral image at 17.5 nm, obtained as the 14th harmonic of the seed (at 245.7 nm, in OPA mode). As shown by the histogram of the FEL energy per pulse (Fig. 5, left), the pulse energy stability is only marginally affected by the higher harmonic order; the standard deviation of the energy per pulse distribution is about 7% while the average relative bandwidth is 0.044%.

2.3. Two-color operation

Understanding the exotic properties of matter driven to extreme non-equilibrium states by interaction with very intense VUV and X-ray pulse has become possible with the advent of ultra-bright FELs. The evolution of such transient states can be monitored developing different photon correlation schemes in which the dynamics triggered by a first 'pump' pulse are probed by a second pulse arriving at a variable delay.

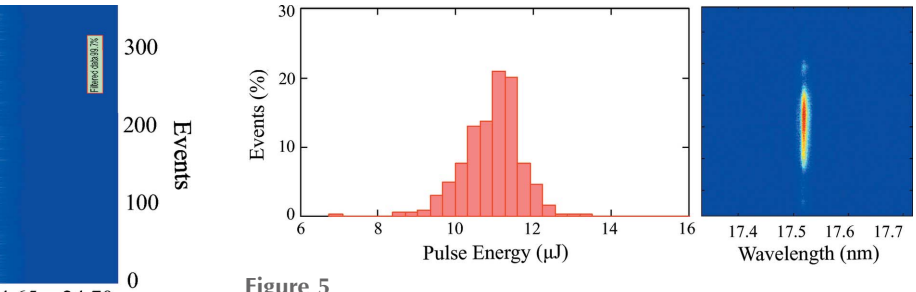

Figure 5
(Left) Histogram of the FEL pulse energy in a sequence of about 330 spectra at 17.5 nm (OPA mode). (Right) Sample spectral image at 17.5 nm. The average relative bandwidth is about 0.044%.

The external seed scheme of FERMI allows the generation of twin pulses by seeding two (temporally) different parts of the electron bunch (Allaria *et al.*, 2013*b*). The two seed pulses can also be at different wavelengths by using slightly different central seeding laser wavelengths, and with a proper delay. The two-electron-bunch seeded regions emit two independent temporally separated FEL pulses at the harmonics of the seed wavelengths, if the separation between the two radiation pulses is inside the bandwidth of the FEL amplification process.

The potential of a twin-pulse seeding scheme to explore transient states of matter, stimulating and probing electronic transitions from core levels, was demonstrated by a pilot pump–probe experiment with Ti grating structure, sketched in Fig. 6. The selected wavelengths of both the pump (λ_1 = 37.2 nm) and probe (λ_2 = 37.4 nm) pulses are within the slope region of the Ti M_2/M_3 absorption resonance, where the Bragg peak intensities are very sensitive to the instantaneous Ti ionization state. The results reported by Allaria *et al.* (2013*b*) and Bencivenga *et al.* (2014) show that, at low intensity (∼mJ cm^{-2}), the diffraction pattern is the unperturbed sum of the 'pump' and 'probe' Bragg intensity. Using a very intense 'pump' pulse, above J cm^{-2}, the diffraction pattern

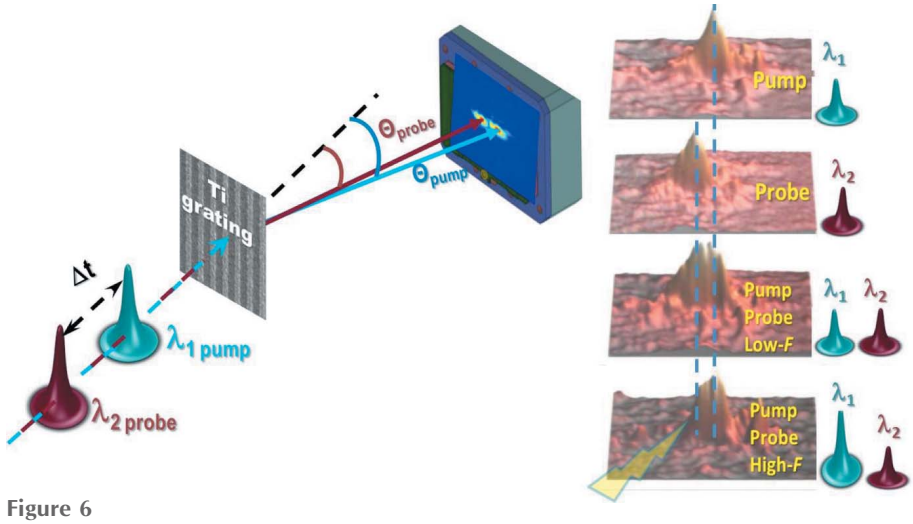

Figure 6
(Left) Two-color FEL pulses, λ_1 and λ_2, tuned across the Ti *M*-resonance, impinge on a Ti grating with a temporal separation Δt. (Right) Diffraction patterns corresponding to single-color 'pump' and 'probe' pulses and to two-color 'pump'–'probe' pulses (delayed by 500 fs) for different flux (F) regimes: low-F = 10–30 mJ cm^{-2}, high-F = 2 J cm^{-2}.

undergoes an abrupt change due to a visible loss of the 'probe' Bragg peak signal. Since the sum of the delay time (∼500 fs) and pulse duration (∼100 fs) is shorter than those of hydrodynamic expansion and ablation, this result can be explained only by dramatic changes in the Ti electronic structure, namely highly ionized states of Ti atoms that push the Ti M_2/M_3 resonance to shorter wavelengths.

In the above scheme the time separation and the relative intensity between these two-colored pulses can be controlled by tuning the delay between the input seed pulses and controlling the laser intensity with a proper attenuator, respectively. The time separation depends on the laser pulse length and on the effective electron bunch extension. Presently the time separation can be varied in the range 300–800 fs.

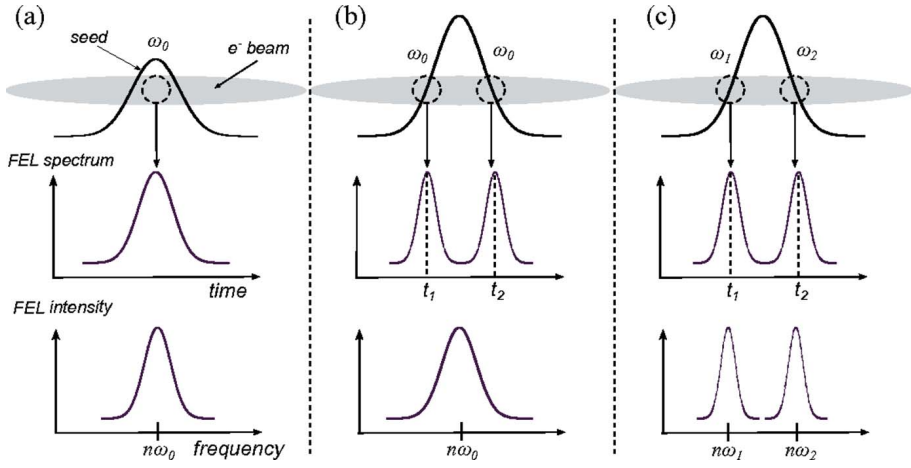

Figure 7
Seed–electron interaction and resulting FEL (temporal and spectral) outputs for different seed configurations: no chirp and moderate seed intensity (*a*), no chirp and high seed intensity (*b*), chirped seed with high intensity (*c*). The meanings of the symbols are explained in the text.

Smaller separations between the pump and probe pulses may be obtained with an alternative scheme where the FEL is driven in deep saturation conditions by seeding the modulator with a powerful laser pulse, also carrying a significant frequency chirp. As a result, the output FEL radiation is split into two pulses, separated in time and having different central wavelengths. The spectral and temporal distances between FEL pulses can be independently controlled, providing the possibility of using the split FEL pulse at the same time as a pump and as a probe (De Ninno *et al.*, 2013).

The concept is sketched in Fig. 7. In standard operation mode (Fig. 7*a*) the seed peak intensity and the strength of the dispersive section, *i.e.* the bunching at the radiator entrance, are tuned to maximize the emission from the part of the electron beam seeded by the center of the Gaussian pulse. The regions of the beam seeded by the tail of the Gaussian pulse arrive instead at the radiator entrance with a not-optimized local bunching factor and the output pulse approximately reproduces the Gaussian shape of the seed, both in time and spectrum. By increasing the seed intensity, while maintaining the strength of the dispersive section, the part of the electron beam that interacts with the center of the Gaussian seed is over-bunched, with a large laser-induced energy spread (Fig. 7*b*). As a result the FEL emission from the center of the bunch is significantly suppressed. The beam portions having optimum bunching (seeded by the outer parts of the Gaussian seed) are the ones before or after this region. As a consequence, the FEL pulse is split in the time domain into two peaks and, if the seed is sufficiently intense to suppress the emission from the central part, by two separated pulses (Labat *et al.*, 2009). If the seed carries a significant frequency chirp (Fig. 7*b*) the two pulses are also characterized by different wavelengths (De Ninno *et al.*, 2013). This opens the possibility to use the FEL as a self-standing source, jitter-free, to carry out two-color pump–probe experiments.

This configuration was extensively investigated at FERMI (Mahieu *et al.*, 2013). As an example we show in the left-hand panel of Fig. 8 the spectral evolution of the FEL pulse measured at the PRESTO spectrometer, as a function of the seed power.

Above a given power threshold the FEL pulse splits, both in time and in spectrum (Gauthier *et al.*, 2013). Larger seed powers correspond to larger extensions of the over-bunched zone around the pulse center and, therefore, to larger temporal and spectral separations. The central and right-hand panels of Fig. 8 show the corresponding (simulated) spectral and temporal pulse splitting. The spectral evolution of the FEL pulse, simulated using the numerical code *PERSEO* (Giannessi, 2006), is in reasonable agreement with experimental data (left-hand panel). The maximum obtainable temporal split is limited by the electron-beam duration and by the possibility of generating long-enough (chirped) seed pulses characterized by significant local power at their tails. This is therefore a complementary technique to the previous one based on seeding the FEL with two independent laser pulses.

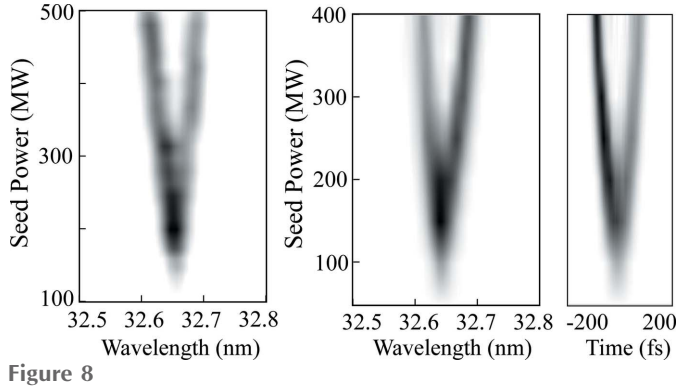

Figure 8
Projected spectral and temporal FEL intensities for different seed powers. Left panel: experimental spectral splitting, measured at FERMI; central and right panels: simulated spectral and temporal splitting (using the code *PERSEO*).

3. FERMI FEL-2

FERMI's FEL-1 has demonstrated the capability of generating light down to 4 nm (Giannessi *et al.*, 2012) and to provide light for experiments down to the Si *L*-edge at 12.4 nm, well below the lower limit of its nominal operation range. However, the FEL performance substantially decays with wavelength when the harmonic conversion order exceeds 12–13. The electron beam's incoherent energy spread at modulator input together with the chromatic dispersion in the radiator limit the maximum practical harmonic upshift ratio for which reasonable microbunching values can be maintained over multiple radiators in a single-stage HGHG configuration (Yu, 1991).

To overcome these limitations, Ben-Zvi *et al.* (Ben-Zvi *et al.*, 1992; Yu & Ben-Zvi, 1997) suggested a 'fresh bunch' alternative two-stage scheme, where the initial radiation seed duration is substantially shorter than the electron beam pulse duration and the interaction in the second stage is shifted on fresh electrons by a strong chicane that delays the electron beam. This temporal delay permits radiation from the first stage to seed a 'virgin' electron beam region that has been unaffected by FEL interaction in the first stage. FEL-2 utilizes this double-stage cascaded HGHG scheme. A schematic layout is shown in Fig. 9. The external laser seeds the first stage, analogous to FEL-1, except for the reduced number of radiators. This stage consists of a modulator (M1) and a two-section radiator (R1); the photon pulse generated in the first stage seeds the second stage, constituted by a second modulator (M2) and six-section radiator (R2). The magnetic chicane after the first stage (DL) delays the electron beam with respect to the photon pulse to shift the seed generated in the first stage onto fresh electrons.

In Fig. 10 we show the spot of the radiation emitted by FEL-2. The output radiation is the superposition of the light emitted by the first and the second stage. The simultaneous presence of the light at the two wavelengths offers the opportunity to perform multicolor experiments where the two harmonic components arrive simultaneously at the sample. Solid-state filters or a gas cell can be used to remove the first-stage output in those cases where it may interfere with the experiment.

3.1. Spectral properties and performances of FEL-2

FEL-2, as FEL-1, is characterized by a high stability of the output central wavelength, and the best energy performance (see Table 2) and spectral quality ($\Delta\lambda/\lambda < 5 \times 10^{-4}$ r.m.s.) are available when the FEL is seeded at fixed wavelength, at the third harmonic of the Ti:sapphire amplifier (261.6 nm). With the OPA laser system the FEL is continuously tunable as

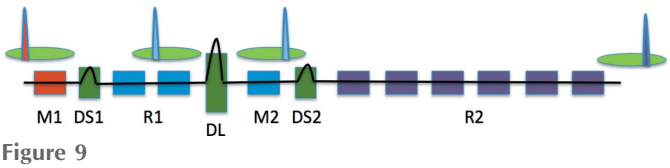

Figure 9
Layout of FERMI FEL-2.

Table 2
List of the main parameters of FEL-2.

Energy per pulse, shot-to-shot stability and relative bandwidth are dependent on the wavelength.

Beam energy (GeV)	1.0–1.5
Peak current (A)	700–800
Repetition rate (Hz)	10–50
Wavelength range (nm)	20–4
Polarization	Variable
Expected pulse length (fs)	<100
Energy per pulse (μJ)	Up to 100 (∼10 @ 4 nm)
Typical relative bandwidth (%, r.m.s.)	∼0.03 (∼0.07 @ 4 nm)
Typical shot-to-shot stability (%, r.m.s.)	∼25% (∼40% @ 4 nm)

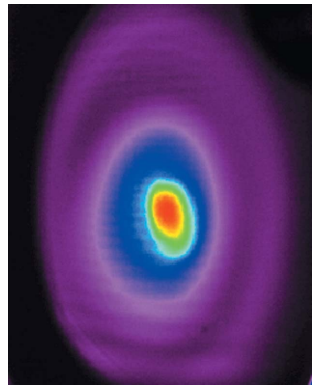

Figure 10
FEL-2. The image represents the FEL spot in false colors from the two stages, superimposed on a YAG screen tilted at 45° with respect to the beam axis. The first-stage spot corresponds to the large blue–magenta ellipse, while the second-stage emission is the small central green–red ellipse. The light from the first stage can be filtered out or used in experiments, depending on the specific requests.

FEL-1. Without adjusting the beam energy, *i.e.* typically during a single user beam-time, the tuning range is approximately ±20%, depending on the required polarization. Typical energy per pulse in the range 10–100 μJ is available, depending on the operation wavelength and polarization. An average energy per pulse of 10 μJ was achieved at 4 nm, the lowest end of the spectral range, only after an accurate machine optimization. A list of the typical FEL-2 parameters is given in Table 2.

A detailed analysis of the spectral properties of the FEL produced by FERMI FEL-2 has been one of the prominent activities during the commissioning stage. As an example we report in Fig. 11 a histogram of the relative line-width measured over a sequence of about 500 spectra at harmonic 48 of the seed, obtained by converting the first stage to harmonic 12 and the second stage to harmonic 4. The figure also shows a single-shot spectral image at 5.4 nm selected from the sequence (center). The FEL emission is characterized by excellent spectral line shapes when the accelerator is carefully tuned for optimal electron beam phase space properties. Also the transverse profile of the FEL pulses is very close to the TEM00 Gaussian mode. Although a similar consideration can be drawn observing the spectrum at 4 nm (right-hand frame in Fig. 11), the FEL tuning at this wavelength is more critical and

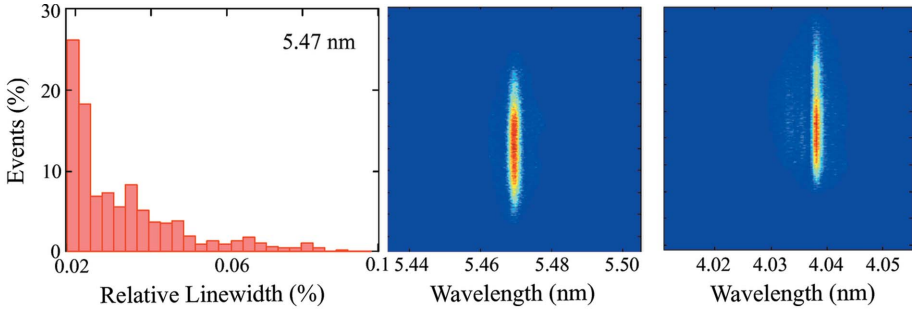

Figure 11
(Left) Histogram of the FEL relative line-width in a sequence of about 500 spectra (95% of the data) for FEL-2 at 5.4 nm. (Center and right) Spectral images of FEL-2 at 5.4 nm and 4.0 nm, respectively. The relative spectral line-widths relevant to the spectral images shown are 0.019% at 5.4 nm and 0.05% at 4.04 nm.

the average line-width of a similar sequence of consecutive shots is a factor of ∼3–4 times larger.

4. Conclusions

FERMI FEL-1 is routinely operating for users. The number of hours dedicated to user experiments has been steadily increasing between 2012 and 2014. FEL-2 has recently achieved the nominal energy per pulse of 10 µJ down to 4 nm. At the end of June 2014 the first user experiment on FEL-2 was carried out. FEL-2 was tuned at the central wavelength of 12.4 nm to study phase transition of Si induced by resonant excitation of the $L_{2,3}$-edge. The wavelength was tuned by ±0.5 to scan the Si edge. The required energy per pulse was around 15 µJ and a relative spectral bandwidth of 5×10^{-4} r.m.s. was provided to the experiment with an uptime of about 85%, quite similar to the value usually obtained on FEL-1. Based upon these encouraging results, we have now opened FEL-2 for user experiments, extending the spectral range of the externally seeded FEL facilities, with their unique properties of longitudinal coherence, into the soft X-ray region.

Acknowledgements

The authors are grateful to all the FERMI team for the valuable support in running the free-electron laser.

References

Allaria, E. *et al.* (2012*a*). *Nat. Photon.* **6**, 699–704.
Allaria, E. *et al.* (2012*b*). *New J. Phys.* **14**, 113009.
Allaria, E. *et al.* (2013*a*). *Nat. Photon.* **7**, 913–918.
Allaria, E. *et al.* (2013*b*). *Nat. Commun.* **4**, 2476.
Allaria, E. *et al.* (2014). *Phys. Rev. X*, **4**, 041040.
Bencivenga, F., Capotondi, F., Casolari, F., Dallari, F., Danailov, M. B., De Ninno, G., Fausti, D., Kiskinova, M., Manfredda, M., Masciovecchio, C. & Pedersoli, E. (2014). *Faraday Discuss.* **171**, 487–503.
Ben-Zvi, I., Yang, K. M. & Yu, L. H. (1992). *Nucl. Instrum. Methods Phys. Res. A*, **318**, 726–729.
Bigot, J.-Y., Vomir, M. & Beaurepaire, E. (2009). *Nat. Phys.*, **5**, 515–520.
Bocchetta, C. J. *et al.* (2007). *FERMI at Elettra FEL Conceptual Design Report.* Elettra-Sincrotrone, Trieste, Italy.
Bonifacio, R., Pellegrini, C. & Narducci, L. M. (1984). *Opt. Commun.* **50**, 373–378.
Capotondi, F., Pedersoli, E., Bencivenga, F., Manfredda, M., Mahne, N., Raimondi, L., Svetina, C., Zangrando, M., Demidovich, A., Nikolov, I., Danailov, M., Masciovecchio, C. & Kiskinova, M. (2015). *J. Synchrotron Rad.* **22**, 544–552.
Capotondi, F., Pedersoli, E., Mahne, N., Menk, R. H., Passos, G., Raimondi, L., Svetina, C., Sandrin, G., Zangrando, M., Kiskinova, M., Bajt, S., Barthelmess, M., Fleckenstein, H., Chapman, H. N., Schulz, J., Bach, J., Frömter, R., Schleitzer, S., Müller, L., Gutt, C. & Grübel, G. (2013). *Rev. Sci. Instrum.* **84**, 051301.
Danailov, M. B., Bencivenga, F., Capotondi, F., Casolari, F., Cinquegrana, P., Demidovich, A., Giangrisostomi, E., Kiskinova, M. P., Kurdi, G., Manfredda, M., Masciovecchio, C., Mincigrucci, R., Nikolov, I. P., Pedersoli, E., Principi, E. & Sigalotti, P. (2014). *Opt. Express*, **22**, 12869–12879.
Dattoli, G., Marino, A., Renieri, A. & Romanelli, F. (1981). *IEEE J. Quantum Electron.* **17**, 1371–1387.
De Ninno, G., Mahieu, B., Allaria, E., Giannessi, L. & Spampinati, S. (2013). *Phys. Rev. Lett.* **110**, 064801.
Eisebitt, S., Lüning, J., Schlotter, W. F., Lörgen, M., Hellwig, O., Eberhardt, W. & Stöhr, J. (2004). *Nature (London)*, **432**, 885–888.
Garcia, G., Nahon, L., Daly, S. & Powis, I. (2013). *Nat. Commun.* **4**, 2132.
Gauthier, D., Mahieu, B. & De Ninno, G. (2013). *Phys. Rev. A*, **88**, 033849.
Giannessi, L. (2006). *Proceedings of FEL 2006 Conference*, pp. 91–94.
Giannessi, L. *et al.* (2012). In *Proceedings of the 2012 FEL Conference*, Nara, Japan. MOOB6.
Haus, H. (1981). *IEEE J. Quantum Electron.* **17**, 1427–1435.
Janssen, M. H. M. & Powis, I. (2014). *Phys. Chem. Chem. Phys.* **16**, 856–871.
Kondratenko, A. M. & Saldin, E. L. (1980). *Part. Accel.* **10**, 207–216.
Labat, M., Joly, N., Bielawski, S., Szwaj, C., Bruni, C. & Couprie, M. E. (2009). *Phys. Rev. Lett.* **103**, 264801.
Mahieu, B., Allaria, E., Castronovo, D., Danailov, M. B., Demidovich, A., De Ninno, G., Di Mitri, S., Fawley, W. M., Ferrari, E., Fröhlich, L., Gauthier, D., Giannessi, L., Mahne, N., Penco, G., Raimondi, L., Spampinati, S., Spezzani, C., Svetina, C., Trovò, M. & Zangrando, M. (2013). *Opt. Express*, **21**, 22728.
Masciovecchio, C. *et al.* (2015). *J. Synchrotron Rad.* **22**, 553–564.
Penco, G., Danailov, M., Demidovich, A., Allaria, E., De Ninno, G., Di Mitri, S., Fawley, W. M., Ferrari, E., Giannessi, L. & Trovó, M. (2014). *Phys. Rev. Lett.* **112**, 044801.
Sasaki, S. (1994). *Nucl. Instrum. Methods Phys. Res. A*, **83**, 347.
Spezzani, C. *et al.* (2011). *Phys. Rev. Lett.* **107**, 084801.
Sprangle, P., Tang, C.-M. & Manheimer, W. M. (1980). *Phys. Rev. A*, **21**, 302–318.
Svetina, C. *et al.* (2015). *J. Synchrotron Rad.* **22**, 538–543.
Tia, M., Cunha de Miranda, B., Daly, S., Gaie-Levrel, F., Garcia, G., Powis, I. & Nahon, L. (2013). *J. Phys. Chem. Lett.* **4**, 2698–2704.
Yu, L. H. (1991). *Phys. Rev. A*, **44**, 5178–5193.
Yu, L. H. *et al.* (2000). *Science*, **289**, 932–935.
Yu, L.-H. & Ben-Zvi, I. (1997). *Nucl. Instrum. Methods Phys. Res. A*, **393**, 96–99.
Zangrando, M., Abrami, A., Bacescu, D., Cudin, I., Fava, C., Frassetto, F., Galimberti, A., Godnig, R., Giuressi, D., Poletto, L., Rumiz, L., Sergo, R., Svetina, C. & Cocco, D. (2009). *Rev. Sci. Instrum.* **80**, 113110.